

# Intracellular Protein Delivery and Gene Transfection by Electroporation Using a Microneedle Electrode Array

Seong-O Choi, Yeu-Chun Kim, Jeong Woo Lee, Jung-Hwan Park, Mark R. Prausnitz,\* and Mark G. Allen\*

*The impact of many biopharmaceuticals, including protein- and gene-based therapies, has been limited by the need for better methods of delivery into cells within tissues. Here, intracellular delivery of molecules and transfection with plasmid DNA by electroporation is presented using a novel microneedle electrode array designed for the targeted treatment of skin and other tissue surfaces. The microneedle array is molded out of polylactic acid. Electrodes and circuitry required for electroporation are applied to the microneedle array surface by a new metal-transfer micromolding method. The microneedle array maintains mechanical integrity after insertion into pig cadaver skin and is able to electroporate human prostate cancer cells in vitro. Quantitative measurements show that increasing electroporation pulse voltage increases uptake efficiency of calcein and bovine serum albumin, whereas increasing pulse length has lesser effects over the range studied. Uptake of molecules by up to 50% of cells and transfection of 12% of cells with a gene for green fluorescent protein is demonstrated at high cell viability. It is concluded that the microneedle electrode array is able to electroporate cells, resulting in intracellular uptake of molecules, and has potential applications to improve intracellular delivery of proteins, DNA, and other biopharmaceuticals.*

Dr. S.-O. Choi, Prof. M. G. Allen  
School of Electrical and Computer Engineering  
Georgia Institute of Technology  
Atlanta, GA 30332, USA  
E-mail: mallen@gatech.edu

Dr. S.-O. Choi, Dr. Y.-C. Kim, Dr. J. W. Lee,  
Prof. M. R. Prausnitz, Prof. M. G. Allen  
School of Chemical and Biomolecular Engineering  
Georgia Institute of Technology  
Atlanta, GA 30332, USA  
E-mail: prausnitz@gatech.edu

Dr. Y.-C. Kim  
Department of Chemical and Biomolecular Engineering  
Korea Advanced Institute of Science and Technology (KAIST)  
Daejeon, 305-701, Republic of Korea

Dr. J.-H. Park  
Department of BioNano Technology and Gachon  
BioNano Research Institute  
Gachon University  
Sungnam, 461-701, Republic of Korea

DOI: 10.1002/sml.201101747



## 1. Introduction

Recent developments in biotechnology have introduced new drugs such as proteins and nucleic-acid-based biotherapeutics to treat a variety of important diseases.<sup>[1]</sup> One of the critical factors for the success of treatment in many cases is effective delivery of the drugs into target cells. This is often difficult to achieve because the cell membrane is not permeable to most drugs. To overcome the cell membrane barrier, researchers have investigated many approaches, including viral vectors and physical methods.<sup>[2,3]</sup>

A promising method for intracellular delivery of target molecules is electroporation, which utilizes an electric field to create short-lived pathways across the cell membrane, through which external molecules can be introduced into cells. Electroporation has been adopted as a common laboratory technique for DNA transfection, clinical use for chemotherapy, and investigational use for gene therapy.<sup>[4]</sup> Also, electroporation has been used to improve DNA vaccination against various diseases, including influenza,

smallpox, and hepatitis B.<sup>[5–7]</sup> However, conventional electroporation procedures cause pain and strong muscle twitching during electric field application due to nerve stimulation; require a high-voltage source to generate sufficient electric field strength for electroporation; and can damage tissue during electroporation due to high electric current.<sup>[8]</sup>

These issues associated with current electroporation procedures may be overcome by adopting microneedles as electrodes for electroporation. In this scenario, a closely spaced array of solid needles measuring hundreds of microns in length is pressed into the skin and used to locally electroporate cells between the needle electrodes. Due to their shallow penetration depth, microneedles can minimize pain during needle insertion. Also, drug injection using a hypodermic needle can be avoided if drug is coated on microneedle electrodes and then dissolved off in the skin. Moreover, the high voltage required to achieve electric fields needed for electroporation can be reduced because of the small gap between microneedles, and the small size of microneedle electrodes can achieve highly localized electroporation, thereby minimizing tissue damage and nerve stimulation during electroporation. Recent studies have shown that electrically conductive microneedles can pierce the skin and electroporate cells for enhanced gene delivery *in vivo*.<sup>[6,9]</sup> However, previous studies have used microneedle electrode devices fabricated either by hand assembly of acupuncture needles or by mechanical micromilling, and have not provided detailed quantification of intracellular uptake of molecules as a function of device operating parameters.

In this study, we sought to develop a microneedle device for electroporation based on a metal-transfer micromolding technique. To achieve electroporation using microneedles, microneedles need to be given electrical functionality by a proper metal-patterning process. Conventional patterning methods based on photolithography are not easy to apply to patterning metal on high aspect ratio microneedles due to the requirement of sample contact to a photomask, which could break the microneedle tips during the process. Here, we adapted a metal transfer process<sup>[10]</sup> using a two-layer micromold to achieve electrical functionality on microneedles. This process allowed forming metal patterns without photolithography on high-aspect-ratio 3D structures such as microneedles during micromolding, which is attractive to fabricate polymer-based microsystems requiring electrical functionality.

In this study, we also sought to provide detailed quantification of intracellular uptake of molecules as a function of device operating parameters using a microneedle electrode array. We therefore quantified uptake of calcein and bovine serum albumin and transfection with DNA, as well as cell viability, as a function of electroporation voltage and pulse length.

Overall, this study provides a novel microfabrication method to produce electrically functional microneedle arrays by metal-transfer micromolding that was shown to transport macromolecules into human prostate cancer cells by electroporation at relatively low voltages. Also, the fabricated

microneedle arrays were inserted into pig cadaver skin without mechanical failure.

## 2. Results and Discussion

### 2.1. Fabrication of Microneedle Electrode Array

The microneedle electrode array was designed for electroporation of tissue surfaces, such as for DNA vaccination in the skin. To achieve this goal, the microneedle array should be both mechanically strong enough to penetrate the skin and electrically functional to generate electric fields required for electroporation. Considering these requirements, we designed a 10-by-10 array of pyramidal-shape microneedles ( $200\ \mu\text{m} \times 200\ \mu\text{m} \times 500\ \mu\text{m}$ ,  $L \times W \times H$ ) with electrical isolation between adjacent microneedles. The gap between microneedles at the base was designed to be  $200\ \mu\text{m}$ . In this way, microneedles with opposite electrical polarity (anodes and cathodes) could be positioned adjacent to each other on the same array. This close spacing provides precise localization of the electric field within the skin and permits relatively low voltages to be used to generate the high electric fields needed for electroporation.

Our first challenge was to develop a method to pattern a metal layer onto the microneedles to provide electrical functionality but also selectively electrically isolate microneedle electrodes from each other. We previously demonstrated a metal-patterned microneedle array for electroporation<sup>[11]</sup> using a laser ablation technique, which is suitable for metallization of high-aspect-ratio structures because it is a non-contact process. However, this process requires precise alignment steps and long processing times for metal patterning. In this study, we present a fabrication method based on a 3D metallization technique that enables formation of 3D metal-patterned microstructures without additional alignment steps for metal patterning.<sup>[12]</sup>

We first prepared an inverse mold by lithography to make a microneedle electrode array. The fabricated SU-8 mold consisted of a 10-by-10 array of tapered square wells, as shown in **Figure 1a,b**. The size of the squares was  $200\ \mu\text{m} \times 200\ \mu\text{m}$  at the base, and the gap between each square was also  $200\ \mu\text{m}$ . The protrusion structure above the wells was designed to isolate adjacent wells; this enabled the electrical polarity of each adjacent electrode pair to be opposite in the final device. For easy and stable removal of the metal on top of the protrusions on the polydimethylsiloxane (PDMS) mold, which is an exact copy of the SU-8 mold, we found that a thick protrusion structure is preferable. In this study, a  $250\ \mu\text{m}$ -thick protrusion structure was prepared to minimize the possibility that metal on a region where metal should reside would be mistakenly removed.

The second question was how to form pointed, deep-trench structures to determine the shape of microneedle tips that need to be sharp for easy insertion into skin. We observed that a blunt-tip microneedle mold is formed as a result of two factors: 1) excessive heat application during the process, which causes undesirable crosslinking of SU-8

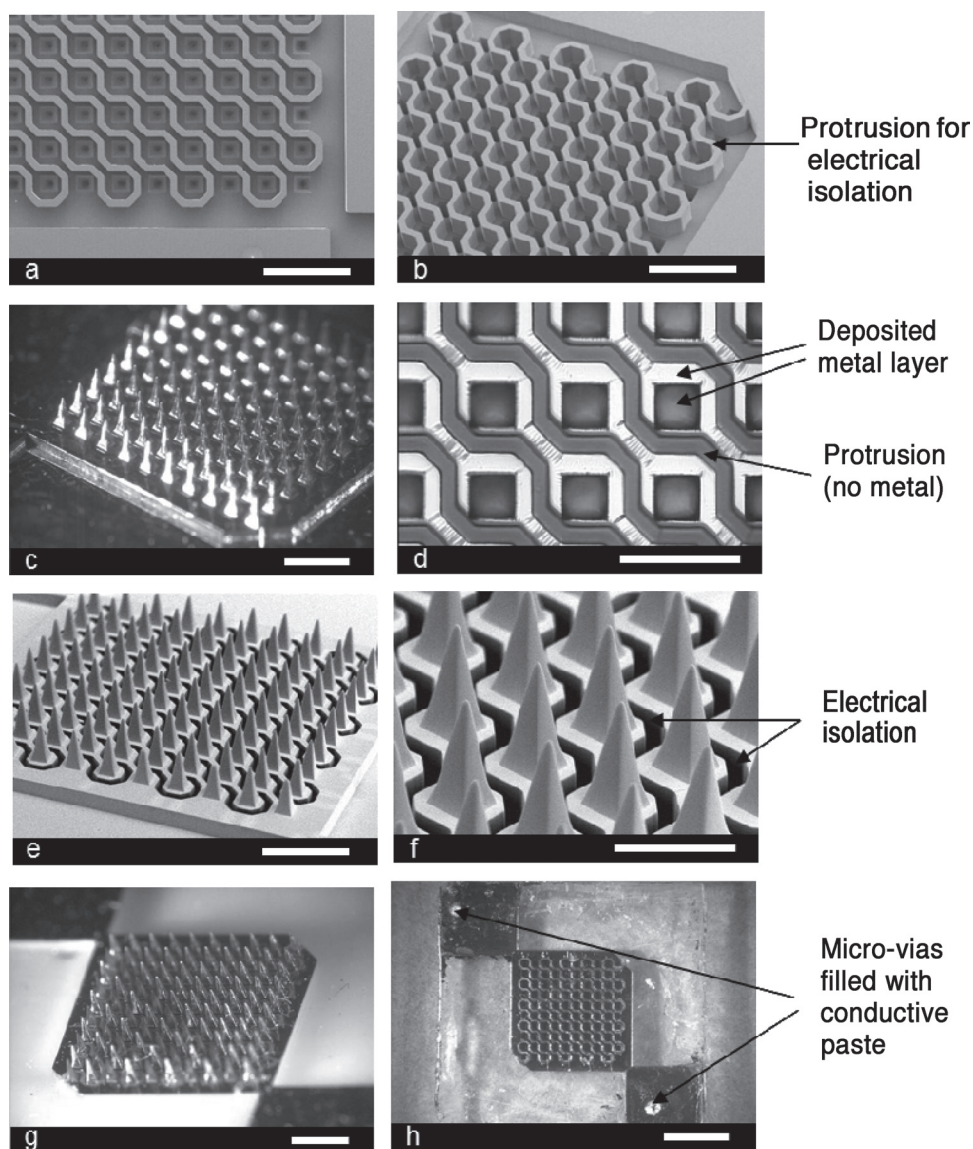


**Figure 1.** Fabricated microneedle array for electroporation. a) Top view of the fabricated SU-8 mold (scale bar: 1 mm). b) Angled view of the SU-8 mold showing the protrusions (scale bar: 1 mm). c) Ni master structure formed by electroplating (scale bar: 1 mm). d) Close-up top view of the PDMS mold replicated from the Ni master after selective removal of metal layer on the protrusions (scale bar: 500  $\mu\text{m}$ ). e) Angled view of the microneedle array, which is formed from the PDMS mold by micromolding, before electroplating (scale bar: 1 mm). f) Further magnified view of the microneedle array showing electrical isolation (dark region) (scale bar: 500  $\mu\text{m}$ ). g) Ni plated microneedle array (scale bar: 1 mm), and h) Backside of the device showing micro-vias filled with conductive polymer (scale bar: 2 mm).

in unexposed areas and 2) incomplete dissolution of pointed trenches during development in a solvent that leaves behind SU-8 in what will become the microneedle tips.

To solve the issue of excessive heat, the second SU-8 layer was spun cast prior to post-exposure baking of the first SU-8 layer, and both layers were baked simultaneously. With this simultaneous baking approach, we were not only able to avoid heat-activated crosslinking in deep trenches but also able to reduce process time.

To facilitate dissolution of uncrosslinked SU-8 in pointed trenches, the sample was placed in a solvent bath to face a vortex of solvent generated by a magnetic stirring bar; thereby saturated solvent in trenches could be replaced with fresh solvent, resulting in the formation of high-aspect-ratio

concave structures. The shape of the mold was confirmed by casting PDMS into the mold and examining the copied PDMS structure under a microscope (data not shown).

From the SU-8 mold, a master structure was subsequently fabricated by Ni electroplating into the mold as shown in Figure 1c. In this study we chose to make the master structure out of metal because of its long life span due to mechanical durability and high temperature resistance, which offers the flexibility of process parameters including material selection and process temperature. The Ni master was separated from the SU-8 mold by etching the Cu seed layer, which was deposited into the SU-8 mold for electroplating.

PDMS was chosen as a micromold material due to its flexibility and low surface energy.<sup>[13]</sup> A PDMS mold replicated

from the Ni master was metallized by electron beam evaporation. After metallization of the PDMS mold with Au/Ti, the metal layers on the protrusions (dark regions between squares) were selectively removed using adhesive tape (Figure 1d). It was observed that micro-wrinkles were formed on the mold, which is believed to be induced by buckling of the deposited metal layers due to thermal expansion/contraction of the PDMS mold during the metallization process.<sup>[14]</sup> However, it turned out that these wrinkles did not affect the electrical continuity of the metal film, which was confirmed by electrical resistance measurement (data not shown).

The patterned metal layer was transferred from the PDMS mold to the polymer structure during micromolding, which formed a metal-patterned microneedle structure. The mechanism of the metal-transfer process is based on the different strengths of adhesion at material interfaces, and typically adhesion strength between PDMS and metal is weaker than that between molding materials and metal, due to the low surface energy of PDMS. Therefore, a metal layer originally residing on the PDMS mold can be transferred to the surface of the molding material during micromolding, which results in the formation of a metal-patterned microneedle array.

We tested different molding materials including polyurethane, UV-curable epoxy and polylactic acid (PLA), and metal transfer occurred for all cases (data not shown), in agreement with literature.<sup>[10,13]</sup> In this study, we chose PLA as a cast material due to its biocompatibility and prior experience in our lab. Figure 1e,f show scanning electron microscopy (SEM) images of the fabricated microneedle arrays, which contain 100 pyramidal-shape microneedles with dimensions of  $200\ \mu\text{m} \times 200\ \mu\text{m} \times 500\ \mu\text{m}$  (L  $\times$  W  $\times$  H). As shown in Figure 1f, adjacent diagonals are separated by a deep trench, which is the reverse structure of the protrusions shown in Figures 1a, 1b, and 1d that provide electrical isolation between diagonals.

The advantage of this metallization process is that it does not require any photolithography or etching steps and enables the patterning of a metal layer on high-aspect-ratio 3D structures with good fidelity. Also, it is compatible with making 3D metal-patterned microstructures out of biocompatible polymers, which is attractive for biomedical applications requiring electrical functionality such as microelectrode arrays for drug delivery as well neural applications and implantable sensors. To apply this metallization process to large-scale production, however, PDMS would not be the best mold material because it cannot be used repeatedly. A potential solution would be to use a metal-mold coated with a thin layer of low-surface energy material such as polytetrafluoroethylene (PTFE).

After applying the transferred metal layer, it was then used as a seed layer for electroplating. Even though the transferred metal layer could be sufficient for implementing the electrical functionality on the final electroporation microneedle structure, Ni was electroplated to thicken the layer in order to confirm electrical connection/isolation between microneedle

electrodes and to form an “etch-stop” layer for laser-drilling holes introduced for electrical connection to the electroporation pulse generator from the backside of the microneedle array. Figure 1g shows the Ni-plated microneedle array, and laser-drilled holes filled with conductive paste are shown in Figure 1h. Although an electrodeposition process was required to prevent the metal layer from damage during the laser-drilling process, this approach may require additional time and cost for device fabrication. Therefore, it is desirable to consider an alternative way to form electrical connections between the microneedle array and pulse generator, which can eventually eliminate the electrodeposition process.

## 2.2. Insertion Test

Because the basic function of microneedles is to cause local electroporation in the skin, electroporation microneedle electrode arrays should be mechanically strong enough to pierce the skin without failure while maintaining electrical functionality.

To test this, we fabricated microneedle devices having a  $5\ \mu\text{m}$ -thick electrodeposited Ni layer, which is thin enough for laser drilling and vacuum filling processes. These microneedle arrays were successfully inserted into pig cadaver skin by hand and exhibited no structural damage even after multiple insertions, as shown in **Figure 2**. We also performed the insertion test with PLA-only (no metal layer) microneedles on pig cadaver skin to examine the mechanical strength of the microneedle itself. After several insertion tests, the PLA microneedles pierced the skin without breakage or bending (data not shown), which indicates that the metal layer only needs to provide electrical, and not mechanical, functionality. This mechanical strength of PLA microneedles is in agreement with previous findings.<sup>[15]</sup>

## 2.3. Electroporation of Cells

We next examined the electrical functionality of the microneedle device to cause electroporation by performing intracellular molecular uptake studies. Calcein, fluorescein isothiocyanate (FITC)-labeled bovine serum albumin (BSA), and plasmid DNA encoding green-fluorescent protein

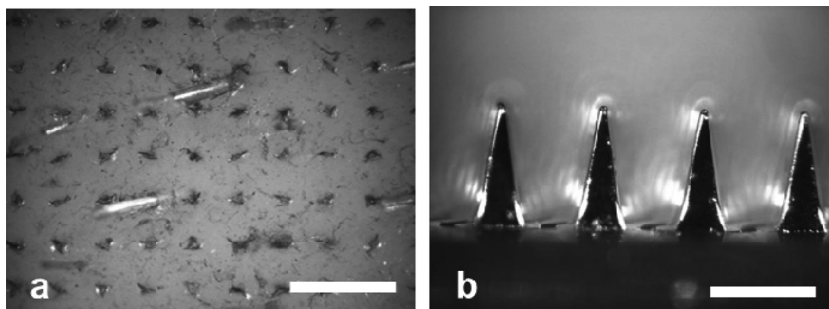


**Figure 2.** Representative optical micrographs of a) pig cadaver skin stained with red tissue-marking dye after removal of a microneedle array from the skin (scale bar: 1 mm) and b) the PLA microneedle array with a  $5\ \mu\text{m}$ -thick electroplated Ni layer after 3 insertion into skin (scale bar:  $500\ \mu\text{m}$ ).

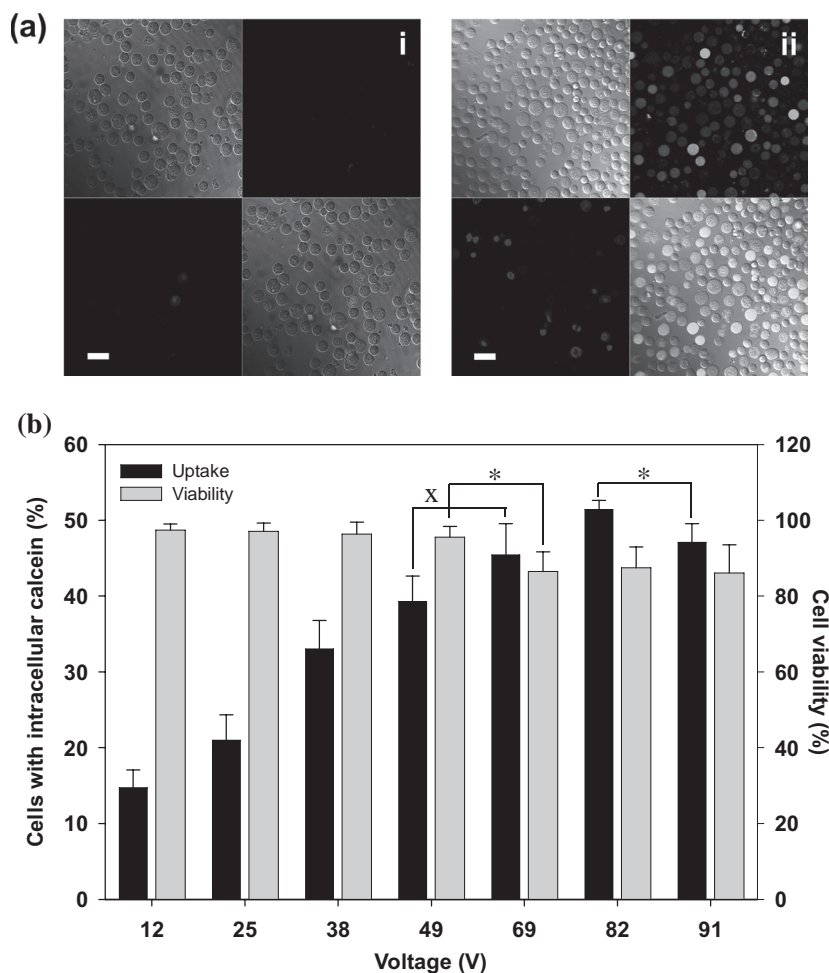


**Figure 3.** Effect of voltage on intracellular calcein uptake after electroporation with a microneedle electrode device. a) Representative confocal microscopic images of human prostate cancer cells after the delivery of calcein by electroporation using a 2.5 ms exponential decay pulse. Each picture contains 4 sections, and each section represents an image taken by a different channel (top left: brightfield, top right: green fluorescence, bottom left: red fluorescence, bottom right: combination of all channels). Cells with intracellular calcein show green fluorescence and dead cells are marked by red fluorescence. Additional images can be seen in Figure S1 in the Supporting Information. i) Unpulsed control, ii) 69 V (scale bar: 50  $\mu$ m). b) Uptake efficiency of calcein and cell viability using 2.5 ms exponential decay pulse at different voltages. Data represent the average of  $n = 3$  replicate experiments. Standard deviation bars are shown. X not significantly different (Student's *t*-test,  $p > 0.05$ ), \* significantly different (Student's *t*-test,  $p < 0.05$ )

(GFP) were chosen as model molecules because they are either fluorescent or encode a fluorescent reporter, which can be easily quantified and imaged. In addition, the effect of molecular weight on uptake efficiency was studied using these molecules due to their large molecular weight difference. The electroporated cells were imaged by multi-photon confocal microscopy, and the fraction of cells with fluorescence was determined quantitatively by flow cytometry.

We first examined the effect of voltage and pulse length on intracellular uptake of a small fluorescent molecule, calcein (623 Da). **Figure 3** shows the extent of uptake after applying exponential decay pulses with a decay time constant of 2.5 ms at different voltages. Microscopy images show that intracellular uptake of calcein, which is indicated by green fluorescence, occurred by electroporation (Figure 3a(ii)),

whereas non-electroporated cells did not contain significant amounts of calcein inside (Figure 3a(i)). The fraction of cells loaded with calcein by electroporation increased until 82 V was applied (analysis of variance, ANOVA,  $p < 0.05$ ) and then slightly decreased at 91 V (Student's *t*-test,  $p < 0.05$ ) (Figure 3b). Approximately half of cells showed intracellular calcein uptake at 82 V.

Cell viability at each voltage condition was also measured (Figure 3b). Up to 49 V, viability was not significantly affected by voltage (ANOVA,  $p > 0.05$ ) and remained greater than 90%. Viability significantly dropped at 69 V (Student's *t*-test,  $p < 0.05$ ), above which viability did not change further (ANOVA,  $p > 0.05$ ) and remained greater than 80%.

The effect of pulse length on uptake efficiency was examined by applying square wave pulses of three different pulse lengths (0.5 ms, 1 ms, or 2 ms) at four different voltages, as shown in **Figure 4**. Intracellular uptake increased with both pulse length and voltage (two-way ANOVA,  $p < 0.05$ ) (Figure 4b). Cell viability was independent of pulse length (two-way ANOVA,  $p > 0.05$ ) and decreased as a weak function of voltage (two-way ANOVA,  $p < 0.05$ ), always remaining above about 90% (Figure 4c).

We next studied uptake of a macromolecule (i.e., BSA) to understand the effect of molecular weight. The pulse conditions were the same as those used for calcein delivery experiments in Figure 3, although the measured applied voltages were slightly higher due to variability in pulse generator performance and/or electrical properties of the microneedle devices. As shown in **Figure 5**, the efficiency of BSA uptake weakly increased as voltage increased up to 56 V

(ANOVA,  $p < 0.05$ ), then jumped higher at 75 V (Student's *t*-test,  $p < 0.05$ ) and plateaued at higher voltages (ANOVA,  $p > 0.05$ ). Maximum BSA uptake was approximately 30%. Cell viability decreased weakly as the applied voltage increased (ANOVA,  $p < 0.05$ ).

Comparing the results of the calcein and BSA experiments (Figure 3 and 5), the uptake efficiency of calcein was higher than that of BSA at a given pulse condition (two-way ANOVA,  $p < 0.05$ ). On average, calcein uptake efficiency was  $2.0 \pm 0.4$  fold greater than BSA uptake at a given pulse condition. This indicates that uptake of small molecules like calcein is easier than macromolecules like BSA. Viability of both groups showed similar results (two-way ANOVA,  $p > 0.05$ ). These findings are consistent with the literature, which has shown in conventional, cuvette-based electroporation

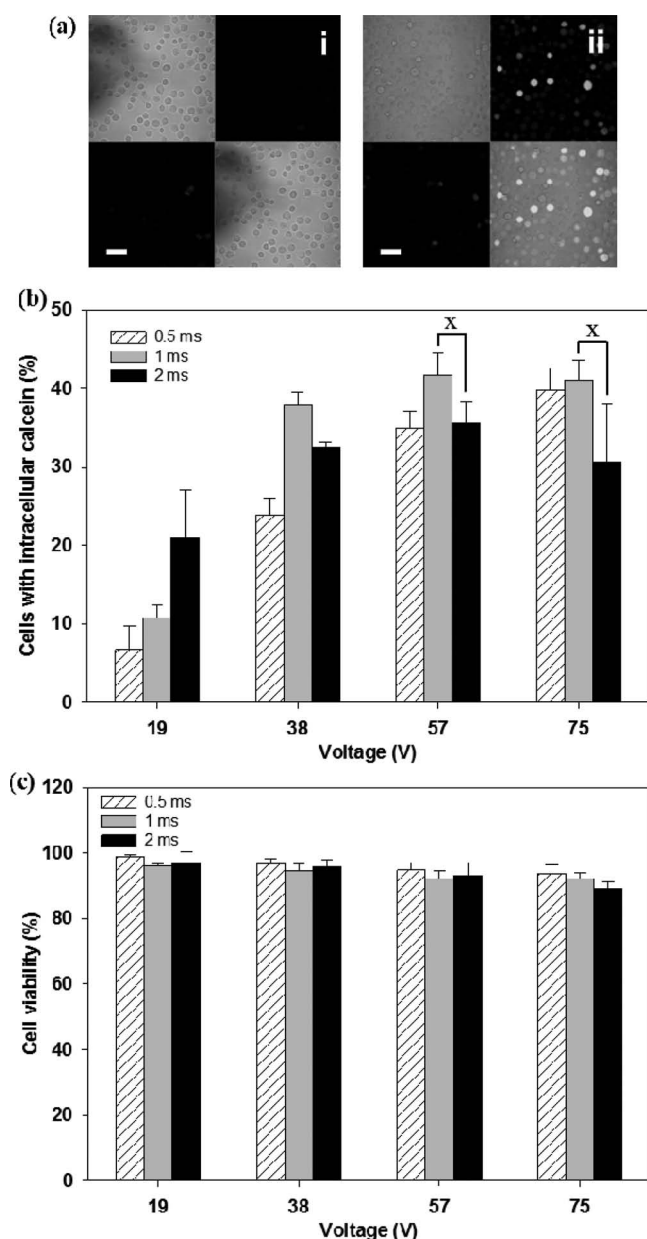


**Figure 4.** Effect of pulse length and voltage on intracellular calcein uptake after electroporation with a microneedle electrode device. a) Representative confocal microscopic images of human prostate cancer cells after the delivery of calcein by electroporation using a 2 ms square wave pulse. Each picture contains 4 sections, and each section represents an image taken by a different channel (top left: brightfield, top right: green fluorescence, bottom left: red fluorescence, bottom right: combination of all channels). Additional images can be seen in Figure S2 in the Supporting Information. i) Unpulsed control, ii) 57 V (scale bar: 50 μm). b) Uptake efficiency of calcein using different pulse length and voltages. c) Cell viability at each pulse condition. Data represent the average of  $n = 3$  replicate experiments. Standard deviation bars are shown. \*not significantly different (Student's *t*-test,  $p > 0.05$ )

i) uptake generally increases with increasing voltage and pulse length, but plateaus at high voltages, ii) viability generally decreases with increasing voltage and pulse length and iii) calcein is taken up more readily than BSA.<sup>[4c,16]</sup>

Because one of the attractive applications of the microneedle electrode array is to deliver genetic material such as DNA into cells in the skin, we assessed the efficiency of DNA transfection of cells using the microneedle electroporation device. Plasmid DNA encoding GFP was tested, and the best efficiency of approximately 12% was obtained at 66 V with a 2 ms square wave pulse, as shown in **Figure 6** (black bar). The transfection efficiency increased with increasing applied voltage (ANOVA,  $p < 0.05$ ). We also measured total green fluorescence intensity, which correlated with total GFP protein expression (Figure 6, gray bar).<sup>[17]</sup> The results indicate that the level of GFP expression increased with increasing applied voltage (ANOVA,  $p < 0.05$ ). These findings are in good agreement with the literature on conventional electroporation.<sup>[4c,18]</sup>

These results further validate the electrical functionality of the microneedle device, which could enable DNA delivery for gene-based therapies or DNA vaccination in skin. The potential advantages of microneedle-based delivery include 1) local administration of DNA into skin with minimal pain, 2) facilitation of DNA uptake locally within the skin, and 3) expected good patient acceptance.

Ideally, electroporation would cause molecular uptake/transfection in all cells with no loss of viability. There is a number of reasons why we did not achieve this ideal goal, such as heterogeneity in cell properties and in the electric field generated by the microneedle electrodes. Microneedles have a tapered design in order to have a sharp tip enabling insertion into skin and a wide base to provide mechanical strength. Thus, the tip-to-tip spacing between diagonally adjacent electrodes was approximately 400 μm, whereas the base edge-to-edge spacing was 200 μm. These and other geometrical features of the microneedles result in a heterogeneous electric field experienced by cells located between the microneedle electrodes. While a tapered shape may be inevitable in microneedle design involving sharp tips, an alternative geometry, such as a parallel-walled microneedle shaft capped by a sharp chisel tip, may reduce these geometrical effects on electric field heterogeneity. Further analysis of microneedle geometry is beyond the scope of this study, but was partially addressed in our previous work.<sup>[11]</sup>

### 3. Conclusion

Previous animal studies have shown that skin electroporation is a promising method for intracellular delivery, especially for DNA vaccines.<sup>[5–7,8b]</sup> This study advanced the field in two ways. First, this study presented a novel microfabrication process to make electrically functional microneedle electrode arrays suitable for electroporation. Previous work in the field has employed conventionally machined and/or hand-assembled devices that have enabled research, but may not be appropriate for large-scale medical application. Here, implementation of electrical functionality to the microneedle array was realized by metal-transfer micromolding, which utilizes surface energy differences between materials to transfer a metallization layer from the PDMS mold to the PLA

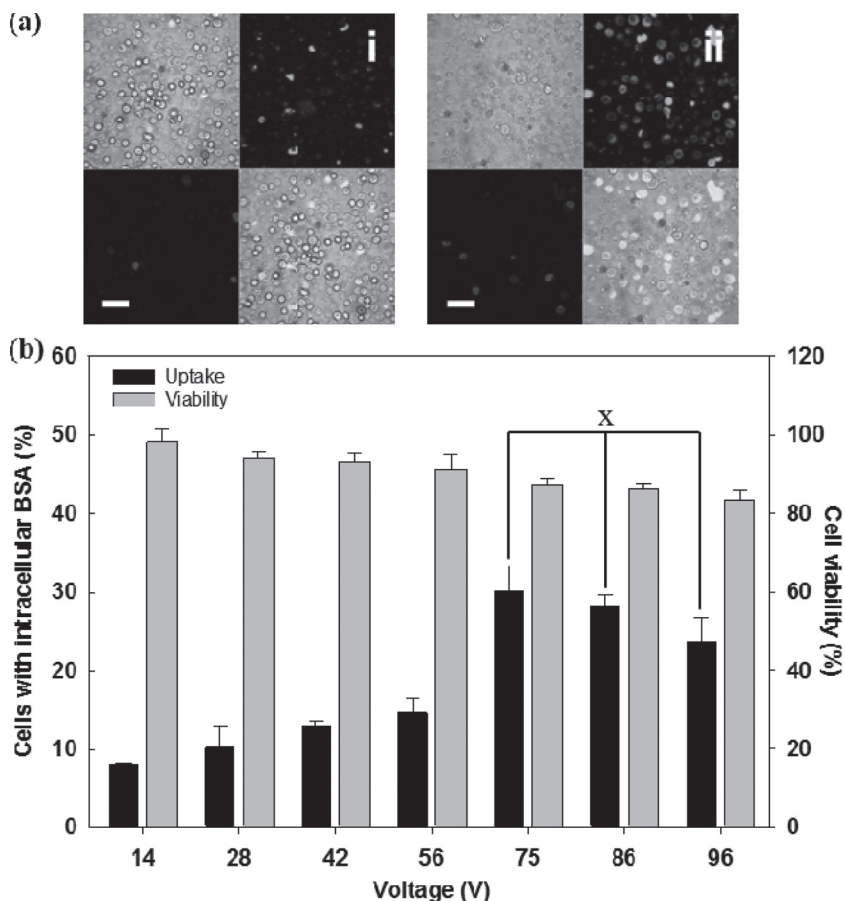


**Figure 5.** Effect of voltage on intracellular BSA uptake after electroporation with a microneedle electrode device. a) Representative confocal microscopic images of the human prostate cancer cells after delivering FITC-BSA using a 2.5 ms exponential decay pulse. Each picture contains 4 sections, and each section represents an image taken by a different channel (top left: brightfield, top right: green fluorescence, bottom left: red fluorescence, bottom right: combination of all channels). Additional images can be seen in Figure S3 in the Supporting Information. i) Unpulsed control, ii) 75 V (scale bar: 50  $\mu\text{m}$ ). (b) Uptake efficiency of BSA and cell viability at different voltages. Data represent the average of  $n = 3$  replicate experiments. Standard deviation bars are shown. \* not significantly different (ANOVA,  $p > 0.05$ )

microneedle device. This technology could also be useful for other biomedical applications requiring metal patterns on 3D structures made from biocompatible materials.

Second, this study carried out the first detailed quantitative analysis of cell electroporation using a microneedle electrode array, showing that intracellular uptake first increased and then plateaued with increasing voltage and increased to a lesser degree with increasing pulse length over the range studied. Relatively efficient uptake of calcein and BSA was demonstrated at high cell viability. DNA transfection was also shown. Microneedle functionality was further addressed by demonstrating mechanical stability of the microneedle arrays through insertion tests with pig cadaver skin.

Overall, this study shows that arrays of microfabricated microneedles can serve as electrodes capable of electroporating cells for uptake of molecules with high viability. These devices can provide a means to perform highly localized, minimally invasive electroporation to deliver proteins, DNA and other compounds into cells for possible applications in

gene-based therapy, DNA vaccination and other applications in biopharmaceutical medicine.

## 4. Experimental Section

**Device Fabrication:** To fabricate the microneedle array for electroporation, a double-layer micromold approach combined with metal-transfer micromolding<sup>[12]</sup> was adopted. The fabrication process consisted of four steps: 1) fabrication of a rigid mold structure using photolithography; 2) fabrication of a master structure from the rigid mold; 3) replication of metal-patterned microneedle arrays using metal-transfer micromolding; and 4) electroplating and formation of electrical interconnects through laser-drilled micro-vias.

**1) Fabrication of the Rigid Mold:** The rigid mold for the microneedle array consisted of two layers and was fabricated using a negative-tone photoresist, SU-8 (SU-8 2025, MicroChem, Newton, MA). The first layer defined the inverse shape of microneedles (Figure 7a), which was formed by inclined lithography,<sup>[19]</sup> and the second layer was formed by conventional UV lithography to define the inverse shape of electrical connections and isolations between microneedles (Figure 7b).

To fabricate an SU-8 mold made of two layers, the first layer of SU-8 was prepared (800  $\mu\text{m}$  thick, 24 h baking at 100  $^{\circ}\text{C}$ ) on a glass substrate, and the inverse shape of the microneedles was formed by exposing the sample through a photomask that had 200  $\mu\text{m}$  square patterns (10-by-10 array) while rotating the sample with inclination under UV light (9000  $\text{mJ cm}^{-2}$ , 20 $^{\circ}$  incident angle).

Then, the second layer was spin coated on top of the first layer, and exposed through a second mask, which was aligned with the first layer to form the inverse shape of the desired metal patterns. Both layers were then developed simultaneously in propylene glycol monomethyl ether acetate (PGMEA) (MicroChem), forming a two-layer SU-8 mold (Figure 7c).

**2) Fabrication of the Master Structure:** To fabricate the master structure, a Ti/Cu seed layer (500  $\text{\AA}$ /5000  $\text{\AA}$ ) was deposited into the SU-8 mold using a CVC DC sputterer (CVC products, Rochester, NY), and Ni was electroplated on top of the Ti/Cu layer at room temperature with a deposition rate of 15  $\mu\text{m h}^{-1}$ . A commercially available Ni plating bath (Watts Nickel, Technic, Cranston, RI) was used for deposition. After a 20 h electrodeposition of Ni into the SU-8 mold, the sample was soaked in copper etchant (saturated  $\text{CuSO}_4$  in  $\text{NH}_4\text{OH}$ ) for 24 h to etch the Cu seed layer, thereby releasing the Ni master from the SU-8 mold upon complete dissolution of the Cu layer (Figure 7d).

**3) Fabrication of the Metal-Patterned Microneedle Array:** A flexible mold was copied from the Ni master by soft lithography.<sup>[20]</sup> PDMS (Sylgard 184, Dow Corning, Midland, MI) was cast onto the

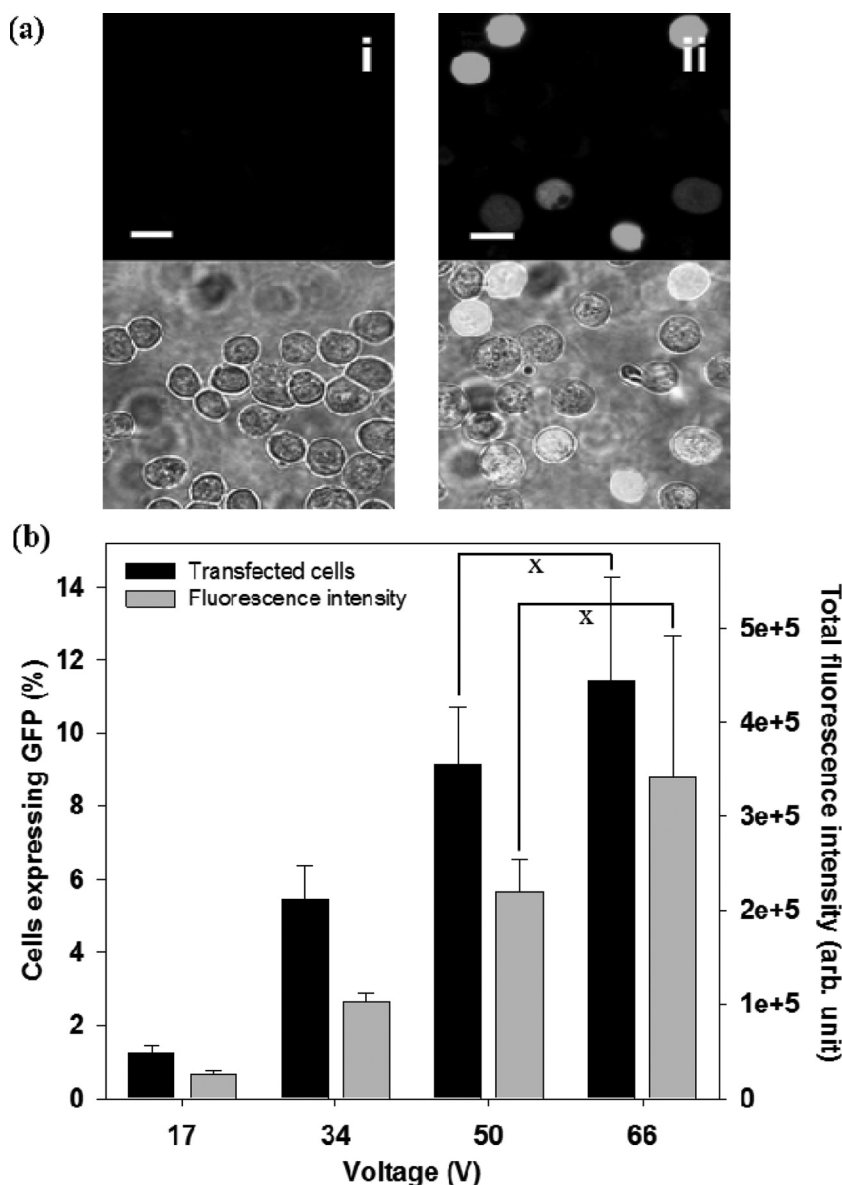


**Figure 6.** Effect of voltage on DNA transfection by electroporation with a microneedle electrode device. a) Representative confocal microscopic images of the human prostate cancer cells at 24 h after intracellular delivery of pDNA expressing GFP using a 2 ms square wave pulse. The top row presents images from the green fluorescence channel showing cells with GFP expression, and the bottom row shows the combination of bright field and fluorescent images. Additional images can be seen in Figure S4 in the Supporting Information. i) Unimpulsed control, ii) 67 V (scale bar: 20  $\mu\text{m}$ ). b) GFP transfection efficiency at different voltages. Black bars represent the percentage of cells expressing GFP and gray bars represent total green fluorescence intensity in cell populations. Data represent the average of  $n = 3$  replicate experiments. Standard deviation bars are shown. \*not significantly different (Student's *t*-test,  $p > 0.05$ )

Ni master placed in a polystyrene (PS) container (2.5 cm  $\times$  2.5 cm  $\times$  0.3 cm, L  $\times$  W  $\times$  H), cured at 37  $^{\circ}\text{C}$  for 24 h, and separated from the master using tweezers. Once the PDMS mold was prepared, the mold was metallized by electron beam deposition (CVC Electron Beam Evaporator, CVC Products) (Figure 7e). After metallization of the PDMS mold with Au/Ti (2000  $\text{\AA}$ /500  $\text{\AA}$ ), adhesive tape was placed on the mold to remove the metal layer on the protrusions above the microneedle mold cavities (Figure 7f). This process was repeated, until the metal layer on the protrusions was completely removed.

Tinker) by applying a vacuum (25 Torr for 1 min). After the filling process, the excess conductive ink was removed, followed by removal of the tape. Once the electrical interconnects were formed, copper wires were attached to the interconnects using silver paste (Figure 7j). For electroporation experiments with cells, the device was firmly attached to a glass slide for convenient handling.

**Skin Insertion Test:** Full-thickness porcine cadaver skin (Pel-Freez, Rogers, AR) was processed by removing subcutaneous fat and hair and was affixed under mild tension to a wooden plate using 1 cm long screws for the test. Procedures were in accordance

After selective removal of the metal layer from the PDMS mold, the target polymer was cast into the mold. In this study, polylactic acid (L-PLA, Birmingham Polymers, Birmingham, AL) was used for device fabrication due to its biocompatibility. For PLA casting, PLA pellets were stacked in the mold and melted in a vacuum oven (1415M, VWR, Radnor, PA) at 195  $^{\circ}\text{C}$  for 1 h. Since the mold contains high-aspect-ratio tapered-well structures, vacuum was applied to fill the mold with PLA (25 torr for 5 min) and the pressure inside the oven was then brought back to atmospheric pressure. The sample was then further melted for 1 h at 195  $^{\circ}\text{C}$  and degassed again to remove any remaining bubbles on the surface of the sample. After degassing, the sample was cooled down to room temperature for 2 h and the molded PLA microneedle structure was separated from the PDMS mold.

During the separation process, the metal layer originally residing on the PDMS mold was transferred to the molded PLA microneedle structure (Figure 7g). The metal patterned PLA microneedle array was further electroplated with Ni to enhance structural rigidity. For Ni electroplating, the sample was attached to a glass slide which bears a pre-deposited Ti/Cu seed layer (300  $\text{\AA}$ /3000  $\text{\AA}$ ). To make an electrical pathway between the sample and the glass slide, silver paste (Think & Tinker, Palmer Lake, CO) was applied to the edge of the sample. Once the silver paste was cured, the glass slide was covered with polyimide tape (3M, St. Paul, MN), except for the sample area where Ni would be deposited. Ni electroplating was performed for 30 min with a 10 mA  $\text{cm}^{-2}$  current density, resulting in the formation of an approximately 5  $\mu\text{m}$ -thick Ni layer (Figure 7h).

To implement an electrical connection to the pulse generator for electroporation, 200  $\mu\text{m}$  diameter micro-vias were drilled from the backside of the device using an excimer laser system (Resonetics, Nashua, NH) (Figure 7i). Before drilling micro-vias, the backside of the device was covered with 25  $\mu\text{m}$ -thick polyimide tape. The micro-vias were then filled with conductive ink (Think &



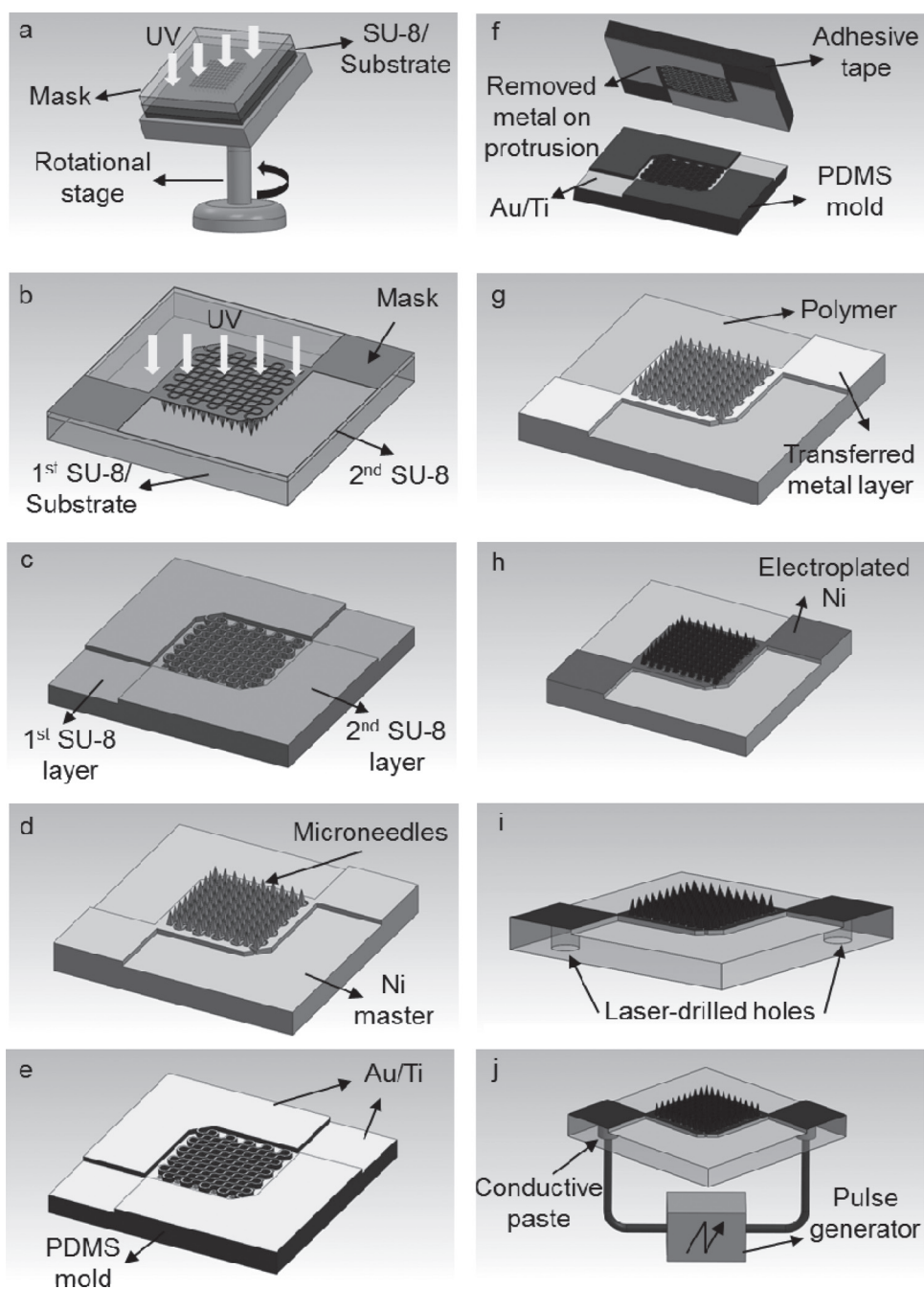


**Figure 7.** Schematic illustration of the fabrication process for an electroporation microneedle array. a) Inclined UV exposure of the first SU-8 layer to form an inverse shape of microneedles. b) UV exposure of the second SU-8 layer to form protrusion structures. c) Formation of a two-layer SU-8 mold by dissolving uncrosslinked SU-8 in PGMEA (refer to Figures 1a and 1b). d) Master structure formation by electrodeposition of nickel into the SU-8 mold and separation from the mold (refer to Figure 1c). e) Metal deposition on the PDMS mold replicated from the master. f) Removal of metal on the protrusion of the PDMS mold (refer to Figure 1d). g) Replication of metal-patterned polymer microneedle array from the PDMS mold by metal transfer micromolding (refer to Figure 1e,f). h) Ni electroplating on the microneedle array (refer to Figure 1g). i) Formation of micro-vias from the backside using laser drilling, and j) Conductive polymer filling into the micro-vias and formation of electrical connection to the outer electronics (refer to Figure 1h).

with the rules of the Georgia Tech Institutional Animal Care and Use Committee. The fabricated microneedle array was placed on this affixed skin and insertion was attempted by applying pressure using the thumb. The array was taken off the wooden plate immediately after the test. A red tissue-marking dye (Shandon, Pittsburgh,

PA), which stains sites of stratum corneum perforation selectively, was applied to the site of insertion and gently cleaned with an isopropanol swab and dry tissue paper after 10 min of exposure. After removal of residual dye, the skin and the tested microneedle array were examined optically (SZX12, Olympus, Center Valley, PA).

**Cell Preparation:** Human prostate cancer cells (DU145, American Type Culture Collection, Manassas, VA) were grown on T-150 flasks (BD Falcon, Franklin Lakes, NJ) as a monolayer in RPMI-1640 medium (Cellgro, Mediatech, Herndon, VA) supplemented with 1% (v/v) penicillin-streptomycin (Cellgro, Mediatech) and 10% (v/v) heat inactivated fetal bovine serum (Atlanta Biologicals, Atlanta, GA) in a humidified condition of 5% CO<sub>2</sub> at 37 °C. The cells were harvested, centrifuged, and resuspended in RPMI-1640 at a concentration of  $2.5 \times 10^6$  cells mL<sup>-1</sup> using a protocol described previously.<sup>[21]</sup> Prostate cancer cells were used in this study, instead of, for example, cells found in the skin, because this cell line has been studied extensively before in our lab for uptake experiments by electroporation and other methods.

**Electroporation Apparatus:** Two types of pulse generator were used for the experiments: an exponential decay pulse generator (BTX ElectroCell Manipulator 600, Genetronics, San Diego, CA) and a square wave pulse generator (Pulse Agile, Cyto Pulse Sciences, Glen Burnie, MD). To apply an electric field, the pulse generator was connected to the microneedle electrode array, and an oscilloscope (TDS 2014B, Tektronix, Beaverton, OR) was also used to examine the actual pulse shape, length, and magnitude in situ.

**Electroporation Protocols:** Calcein (Invitrogen, Carlsbad, CA), FITC-tagged BSA (Sigma-Aldrich, St. Louis, MO), and a plasmid DNA encoding GFP (gWizTM-GFP, Aldevron, Fargo, ND) were used as model molecules. Each molecule type was added to the cell suspension and homogeneously mixed by vortexing. The final concentrations of calcein, BSA, DNA were 30 μM, 25 μM, and 100 μg mL<sup>-1</sup>, respectively. Prior to electroporation, a volume of 6 μL of this suspension was applied as a hemispherical droplet over the microneedle array. After applying voltages using the pulse generator, the cells were collected in microcentrifuge tubes. For each experimental condition, 10 experiments were performed and pooled to collect enough cells for analysis. Each experimental condition was repeated three times and the results were averaged.

After electroporation, the collected samples were incubated in a water bath at 37 °C for 10 min, which allowed the cells to recover, and were then washed with phosphate-buffered saline (PBS) and centrifuged (3500 g, 5 min, Eppendorf, Westbury, NY) three times to remove extracellular model molecules in the supernatant. In the case of calcein and BSA delivery experiments, the washed cell samples were resuspended in a final volume of 200 μL of PBS containing 15 μM propidium iodide (PI, Invitrogen), a viability marker that stains nonviable cells with red fluorescence. The samples with pDNA were further incubated after electroporation in complete cell culture medium in a humidified condition of 5% CO<sub>2</sub> at 37 °C for 20 h, followed by the same sample preparation steps as those of calcein and BSA, except PI staining was not done.

In the BSA delivery study, it was observed that residual BSA was still on the cell membrane after washing with PBS. Due to the residual BSA on the cell membrane, green fluorescence was detected in the control sample during flow cytometry analyses. To remove this artifact, the percentage of cells that appeared to have uptake in the control samples, which was due to the surface BSA, was subtracted from the percentage of uptake in each electroporated sample.

**Flow Cytometry:** The uptake of fluorescent molecules, DNA transfection efficiency, and cell viability were measured by a BD LSR benchtop flow cytometer (BD Biosciences, San Jose, CA), and data were analyzed by FCS Express V3 (De Novo Software, Los

Angeles, CA). Each analysis sampled approximately 20 000 cells using methods described previously.<sup>[21]</sup> Briefly, the cellular uptake and transfection efficiency were determined by the fraction of cells with green fluorescence intensity greater than the background intensity of non-electroporated cells. Similarly, red fluorescence intensity due to PI staining was used to determine the fraction of nonviable cells among the total cell population.

**Multiphoton Confocal Microscopy:** The cell samples were visually analyzed using a multi-photon confocal microscope (Zeiss LSM 510, Carl Zeiss Microimaging, Thornwood, NY). Five microliters of the cell sample was placed on a 25 mm glass microscope cover slip and imaged using 40× or 100× oil-immersion objectives.

## Supporting Information

Supporting Information is available from the Wiley Online Library or from the author.

## Acknowledgements

The authors would like to thank Dr. Robyn Schlicher and Mr. Joshua Hutcheson for helpful discussions regarding flow cytometry analysis, Dr. Ying Liu for guiding the DNA transfection study, Mr. Winston Pewin for drawing 3D schematics, and Ms. Donna Bondy for administrative support. This work was carried out at the Institute for Bioengineering and Bioscience; Center for Drug Design, Development and Delivery; and Microelectronics Research Center at Georgia Tech. This study was supported in part by National Institutes of Health. M.R.P. and M.G.A. serve as consultants and are inventors on patents licensed to companies developing microneedle-based products. M.R.P. is a founder/shareholder of companies developing microneedle-based products. For this reason, this study could affect personal financial status. This potential conflict of interest has been disclosed and is overseen by Georgia Tech and Emory University.

- [1] a) M. A. Kutzler, D. B. Weiner, *Nat. Rev. Genet.* **2008**, *9*, 776–788; b) J. A. Engelman, *Nat. Rev. Cancer* **2009**, *9*, 550–562.
- [2] I. M. Verma, M. D. Weitzman, *Annu. Rev. Biochem.* **2005**, *74*, 711–738.
- [3] S. Mehier-Humbert, R. H. Guy, *Adv. Drug Deliv. Rev.* **2005**, *57*, 733–753.
- [4] a) M. J. Jaroszeski, R. Heller, R. A. Gilbert, *Electrochemotherapy, Electrogenetherapy, and Transdermal Drug Delivery*, Humana Press, Totowa, NJ, **2000**; b) J. Gehl, *Methods Mol. Biol.* **2008**, *423*, 351–359; c) A. G. Pakhomov, D. Miklavcic, M. S. Markov, *Advanced Electroporation Techniques in Biology and Medicine*, CRC Press, Boca Raton, FL, **2010**; d) M. Breton, L. M. Mir, *Bioelectromagnetics* **2012**, *33*, 106–123.
- [5] M. W. Chen, T. J. R. Cheng, Y. X. Huang, J. T. Jan, S. H. Ma, A. L. Yu, C. H. Wong, D. D. Ho, *Proc. Natl. Acad. Sci. USA* **2008**, *105*, 13538–13543.
- [6] J. W. Hooper, J. W. Golden, A. M. Ferro, A. D. King, *Vaccine* **2007**, *25*, 1814–1823.
- [7] A. Luxembourg, D. Hannaman, B. Ellefsen, G. Nakamura, R. Bernard, *Vaccine* **2006**, *24*, 4490–4493.

- [8] a) A. Gothelf, L. M. Mir, J. Gehl, *Cancer Treat. Rev.* **2003**, *29*, 371–387; b) S. Babiuk, M. E. Baca-Estrada, M. Foldvari, M. Storms, D. Rabussay, G. Wiedera, L. A. Babiuk, *Vaccine* **2002**, *20*, 3399–3408; c) T. E. Tjelle, R. Salte, I. Mathiesen, R. Kjekken, *Vaccine* **2006**, *24*, 4667–4670; d) M. R. Prausnitz, *Adv. Drug Delivery Rev.* **1996**, *18*, 395–425.
- [9] a) L. Daugimont, N. Baron, G. Vandermeulen, N. Pavselj, D. Miklavcic, M. C. Jullien, G. Cabodevila, L. M. Mir, V. Preat, *J. Membr. Biol.* **2010**, *236*, 117–125; b) K. Yan, H. Todo, K. Sugibayashi, *Int. J. Pharm.* **2010**, *397*, 77–83.
- [10] S. H. Hur, D. Y. Khang, C. Kocabas, J. A. Rogers, *Appl. Phys. Lett.* **2004**, *85*, 5730–5732.
- [11] S.-O. Choi, Y. C. Kim, J. H. Park, J. Hutcheson, H. S. Gill, Y. K. Yoon, M. R. Prausnitz, M. G. Allen, *Biomed. Microdevices* **2010**, *12*, 263–273.
- [12] S. Rajaraman, S.-O. Choi, M. A. McClain, J. D. Ross, M. C. LaPlaca, M. G. Allen, *J. Microelectromech. Syst.* **2011**, *20*, 396–409.
- [13] D. W. V. Krevelen, *Properties of Polymers*, Elsevier, Amsterdam, **1997**.
- [14] N. Bowden, S. Brittain, A. G. Evans, J. W. Hutchinson, G. M. Whitesides, *Nature* **1998**, *393*, 146–149.
- [15] J. H. Park, M. G. Allen, M. R. Prausnitz, *J. Controlled Release* **2005**, *104*, 51–66.
- [16] M. R. Prausnitz, B. S. Lau, C. D. Milano, S. Conner, R. Langer, J. C. Weaver, *Biophys. J.* **1993**, *65*, 414–422.
- [17] M. R. Soboleski, J. Oaks, W. P. Halford, *FASEB J.* **2005**, *19*, 440–442.
- [18] P. J. Canatella, M. R. Prausnitz, *Gene Ther.* **2001**, *8*, 1464–1469.
- [19] M. Han, W. Lee, S. K. Lee, S. S. Lee, *Sens. Actuators, A.* **2004**, *111*, 14–20.
- [20] Y. N. Xia, G. M. Whitesides, *Annu. Rev. Mater. Sci.* **1998**, *28*, 153–184.
- [21] P. J. Canatella, J. F. Karr, J. A. Petros, M. R. Prausnitz, *Biophys. J.* **2001**, *80*, 755–764.

Received: August 25, 2011  
Revised: October 17, 2011  
Published online: February 13, 2012